Alternative Route for the Preparation of Zr – doped TiO_2 photoanodes for Dye – Sensitized Solar Cells (DSCs)

Riccardo Bendoni[a,b,*], Elisa Mercadelli[a], Nicola Sangiorgi[a,b], Alberto Strini[c], Alex Sangiorgi[a,d] and Alessandra Sanson[a]

[a] Institute of Science and Technology for Ceramics – National Research Council of Italy (ISTEC-CNR), via Granarolo, 64 - I-48018 Faenza (RA) – Italy.

[b] Department of Chemical Science and Technologies and NAST center University of Rome Tor Vergata, via della Ricerca Scientifica, 00133 Rome, Italy

[c] Construction Technologies Institute – National Research Council of Italy (ITC-CNR) via Lombardia, 49 - I-20098 San Giuliano Milanese (MI) – Italy

[d] Department of Chemistry , University of Parma, Parco Area delle Scienze, 23/A, 43124 Parma □ Italy.

*Corresponding author. CNR-ISTEC, Institute of Science and Technology for Ceramics, National Research Council, Faenza 48018, Italy. Tel.: +39 0546 699776; fax: +39 0546 46381.

E-mail address: riccardo.bendoni@istec.cnr.it

Abstract

In this study, a novel procedure for the production of Zr-doped TiO_2 ceramic layers, deposited by screen-printing technique, is presented. A suitable Zr precursor (Zr (IV) 2,4 pentanedionate) was added to the formulation of a standard TiO_2 ink, in order to promote the diffusion of Zr ions directly during the sintering of the deposited layers. In order to evaluate the impact of this process on the properties of the ink, thermal and rheological analysis were done; a significant effect on the flow behavior was found, related to a relevant dispersing action of the precursor. The efficacy of the method was proven by XRD analyses, that showed the stabilization of anatase phase and crystal size at high temperature (700°C), due to Zr doping. The properties of the films were then analyzed in order to evaluate their application as photoanodes for Dye-Sensitized Solar Cells (DSCs). The use of the Zr precursor resulted to improve the film morphology, whereas it did not affect the dye adsoption capability of the TiO_2. Electrochemical characterization pointed out increased flat band potential and density of states (DOS), both meaning a potential enhancement of the final device performances. Finally, the proposed doping method resulted effective and potentially adaptable to other dopant-semiconductor systems.

Keywords

Zr-doped TiO_2 photoanodes, Screen printing, Dye-sensitized solar cells, Anatase stabilization.

1. Introduction

Since their invention in 1991 by Grätzel and O'Regan [1], Dye – Sensitized Solar Cells (DSCs) have attracted a great interest due to the use of environmental friendly materials and the simple and low cost manufacturing process. In the last two decades several efforts have been made in order to improve the performances of DSCs, leading to a record efficiency of 13.0% for the standard configuration [2]. In this model the cell is composed of a photoactive dye adsorbed onto a mesoporous film made of a wide band gap semiconductor, functioning as the photoanode; the device is then completed by a liquid electrolyte and a platinum coated counter electrode. Among these components the photoanode plays the crucial roles of collecting and transporting charges from the excited dye to the external circuit [3]. Since the initial cell configuration of 1991, TiO_2 has constantly given the best performance for this application, and several studies have been conducted to further increase its properties, for example by suppressing charge recombination or improving the interfacial charge transfer. One of the most promising pathways followed is the modification by doping with different ions[4]. Non-metals like N, F, Ca, B [5-8], and metal elements such as Zn, Mg, Sn, Nb, Ce and Zr [9-13] have been reported to effectively endow specific properties to the photoanode, with clear benefits on the cell performances. The insertion of Zr^{4+} ions in TiO_2 lattice in particular has been related to an increase in V_{OC}, due to a negative shift in the conduction band edge; moreover a reduction of the recombination rate was observed [4,13-15], not necessarily including the Zr in the TiO_2 lattice but just by covering TiO_2 particles with a few nanometers thick ZrO_2 passivating shell [16].

Several techniques have been reported for the preparation of doped TiO_2, such as co – precipitation, incipient wet impregnation, mechanochemical doping, hydrothermal crystallization, chemical vapor deposition and sol – gel [4-15]. Nevertheless all the above-mentioned methods require time and energy consuming processes, as well as a strict control of the operating conditions; these factors could have a negative impact on the cost -effectiveness of DSCs manufacturing process.

The aim of this study was the development of an alternative route for the rapid and efficient doping of TiO_2 with Zr^{4+}, when used for the screen printing deposition of the photoanode layer.

A commercial nano - sized TiO_2 (Aeroxide Degussa P25) based screen printing ink was realized by adding a Zr precursor (Zr (IV) 2, 4 pentanedionate) directly into the formulation. This process was chosen in order to promote the in – situ diffusion of Zr^{4+} ions into TiO_2 crystal lattice, directly during the sintering of the deposited film, avoiding any additional thermal or purification step. Two different techniques were also considered for comparison, involving a powder impregnation procedure and a mixture of ceramic oxides, in order to investigate other possible doping procedures realized through the modification of the screen-printing ink formulation. The properties of the obtained systems were compared with the ones of a pure TiO_2 ink considered as reference. The effects of the proposed doping technique on the rheology and thermal properties of the inks and on the microstructure and electronic properties of the corresponding films were assessed, in order to evaluate the suitability of the presented method for the production of doped DSC photoanodes and its possible impact on the performances of the cells.

2. Materials and method

2.1 Preparation of screen-printing inks

Ink P25 was prepared using commercial powders (Degussa P25 Aeroxide, Germany, average particle size 21 nm) mixed with a dispersant, an organic solvent (terpineol, Sigma - Aldrich), a soluble binder (ethyl cellulose, EC, Sigma - Aldrich) and a plasticizer (Table I).

Table I. Composition of P25 ink

Component	Volume fraction (%)
TiO_2 P25 Aeroxide	8.0
Dispersant	0.7
Terpineol	88.5
EC	1.2
Plasticizer	1.6

The system was mixed by ball milling using ZrO_2 grinding media, and then milled in a three roll mill equipped with ZrO_2 rollers (Exakt 80E, Exakt, Nordestedt, Germany) in order to homogenize the ink and infer the proper rheological properties.

The novel doping procedure was developed by dissolving Zr (IV) 2,4 pentanedionate (Alfa Aesar, Germany) in terpineol and adding the solution to the TiO_2 suspension; the resulting ink was labelled as TZ1. Two additional possible doping methods were performed with the following procedures. The first (ink TZ2) implied the impregnation of P25 particles through ball milling (24 h) in ethanol (99,8%, Sigma-Aldrich, Germany) followed by a drying step, while the second (ink TZ3) was realized mixing TiO_2 and ZrO_2 (TOSOH, Japan, d < 200 nm) powders. All the compositions retained the same ratios of TiO_2 and organic components reported in Table I. The considered amount of Zr used as dopant was fixed at 1% mol for each procedure.

2.2 Photoanode deposition

The inks were deposited onto Fluorine – doped Tin Oxide (FTO) glass substrates (sheet resistance 7 Ω/sq, Solaronix, Switzerland) using a semi-automatic screen-printer (AUR'EL 900, AUR'EL Automation s.p.a., Italy). The thickness of each layer of an area of 1 cm^2 was adjusted to approximately 8 μm. Deposited films were dried in air at room temperature and subsequently treated in static air at 450°C for 30 minutes. The same thermal treatment was conducted on samples of each ink, to obtain calcined powder for a more complete characterization.

2.3 Characterizations

Rheological measurements were performed using a controlled stress rotational rheometer (Bohlin C-VOR 120, Bohlin, Malvern, UK), equipped with serrated plates (diameter = 25 mm). All the measurements were performed at 25 °C setting the distance between the plates at 500 μm.

Thermal analyses (TG/DSC, STA 449 Netzsch Geraetebau GMbH, Selb, Germany) were performed to study the evolution of Zr precursor in air and the organic burn – out of the inks.

The X – ray diffraction data were obtained using a Bruker D8 diffractometer (Germany), in the 10 – 80° range (step 0.02°). Specific surface area of the powders were obtained applying the Brunauer – Emmett – Teller (B.E.T.) single point method (Sorpty 1750, Carlo Erba, Milan, Italy). Diffuse reflectance spectroscopy analyses were conducted using a Perkin Elmer Lambda 35 spectrophotometer equipped with a Labsphere SRS – 99 – 010 integrating sphere, in order to measure the band gap energies of the samples.

Dye loading was evaluated sensitizing the films with a solution of cis-diisothiocyanato-bis(2,2'–bipyridyl-4,4'-dicarboxylato)-Ruthenium(II) bis (tetrabutylammonium)

(Sigma-Aldrich, Germany), known as N719 dye, (0.3 mM in absolute ethanol) for 15 hours, and then desorbing the dye using a NaOH 0.1M aqueous solution.

The morphology of the TiO_2 films were analyzed by field emission gun - scanning electron microscope (FE – SEM, ΣIGMA: Zeiss, Germany), equipped with energy dispersive X – ray spectroscopy (EDS) system.

Electrochemical measurement were conducted in a conventional three electrodes cell using a saturated calomel electrode as reference (SCE, AMEL electrochemistry, Italy) and a platinum wire as counter electrode. Cyclic voltammetry (CV) analysis were done in aqueous H_2SO_4 solution (pH 3). Flat band potentials were determined through electrochemical impedance spectroscopy (EIS) using Mott – Schottky equation. Potential range was set between -1 V and + 1 V with perturbation amplitude of 10mV in the frequency range 10 KHz to 100 Hz. 0,1 M $LiClO_4$ aqueous solution was used as electrolyte. CV and EIS were carried out using Autolab PGSTAT302N with an internal frequency response analyzer (Eco Chemie, The Netherlands).

3. Results and discussions

3.1 Inks characterization

The optimal precursor for the proposed process has to be compatible with the solvents used (terpineol and ethanol, the latter used for the powder impregnation in TZ2 ink) and have a negligible moisture sensitivity, in order not to be rapidly degraded. Among the commercially available compounds meeting these requirements, Zr (IV) 2, 4 pentanedionate was chosen, considering his relatively lower toxicity. An additional requisite, strictly related to the manufacturing of the photoanode of a DSC, is an adequate thermal behavior. TiO_2 layers used for this application are in fact generally

sintered at 450°C, to maintain the maximum amount of anatase phase, which is the most favorable, preventing the phase transition to rutile. The organic part of the precursor therefore has to be completely degraded at this temperature, in order to avoid the presence of post-sintering residues that could affect the electronic properties of the photoanode and its affinity with the other components of the cell.

The thermal evolution of the precursor was then evaluated by performing TG/DSC analysis in air; the results are reported in Figure 2.

The DSC curve shows an endothermic peak at 195°C and an exothermic one around 380°C, responsible of the global weight loss of 75% due to the degradation of the organic components of the precursor. After 400°C no additional weight losses are observed, even if broad endothermic and exothermic peaks are clearly visible. These transitions could be related to the crystallization of ZrO_2, at around 600°C, and to the formation of a metastable monoclinic phase [17-19]. This result indicates that the temperature considered for the sintering of the deposited films (450°C) will ensure the complete burnout of the organic part of the precursor, therefore it is completely suitable for the development of the doping process. Ink TZ1 was then prepared following the methods schematized in Figure 3.

The precursor solution was added to the TiO_2 suspension, afterwards the formulation was completed by adding the binder. In this procedure the TiO_2 powders are initially functionalized with the dispersant, in order to assure an efficient particle dispersion, and then the Zr precursor is added. This method was chosen in order to avoid any powder treatment or intermediate step.

On the contrary, for the production of ink TZ2, TiO_2 powders were firstly functionalized with the precursor and then dried, before adding the other components of

the ink. This intermediate step was included in order to simulate a more conventional "impregnation-like" procedure, thus avoiding high temperature treatments of the powders. Following this procedure, the TiO_2 is firstly covered by Zr (2, 4 pentanedionate) molecules, and only in a second time by the dispersant; the impact of these different approaches on the properties of the inks and on the corresponding ceramic layers will be considered. Finally, the analysis of TiO_2 and ZrO_2 considered as a mixture of ceramic oxides, compared to the previous systems, was at the basis of ink TZ3. The amount of Zr^{4+} was set at 1% mol for each system, since it has been proved to have a significant influence on the electronic properties of TiO_2 both in photovoltaic and photocatalytic applications [13,14,20,21]; in addition it generally does not originate undesired ZrO_2 phase segregation, that is useful for the preliminary study of a new doping procedure.

In order to characterize the properties of the inks, TG/DSC analysis were initially done, focusing on the impact of the precursor molecules (inks TZ1 and TZ2) and of the secondary ZrO_2 phase (ink TZ3) on the thermal behavior of the inks.

Figure 4 shows the TG/DSC obtained for ink TZ1. The transitions related to the decomposition of Zr (IV) 2,4 pentanedionate are no more visible, covered by the largely higher amount of organics included in the formulation. Moreover no dissimilarities in the thermal behavior were found among the different inks, as a consequence of the low amount of additional organics (TZ1 and TZ2) or ZrO_2 powder introduced in the formulations.

More significant differences between the systems studied arose from the analysis of their rheological behavior. Viscosity measurements were performed by sweeping over 23 values of shear rate, between 0.002 and 200 s^{-1}. For each measurement, a pre-shear of 2 minutes at 0.01 s^{-1} was first applied for the system to reach equilibrium, then the

shear rate was increased up to 200 s^{-1} and then sequentially decreased down to 0.002 s^{-1}, to simulate the change of shear induced by the printing process. Figure 5 reports the flow curves obtained for each ink.

The systems exhibit a pseudoplastic behavior, in which the viscosity decreases by increasing the shear rate and recovers, with different degrees of hysteresis, after the inverse cycle. P25 and TZ3 show almost overlapping curves, suggesting that the addition of ZrO_2 as oxide, in this low percentage, does not influence the rheology of the ink, as it does not affect the surface of TiO_2 and therefore its interaction with the organic components. Both systems denote high starting values of viscosity and an almost linear dependence on the shear rate, in addition a small variation is registered between the values of viscosity of the upward and downward curves. This behavior is a consequence of an highly structured and reticulated powder – binder network, resulting in a reduced effect of the shear applied by the rheometer on the microstructural changes of the ink [22]. On the other hand TZ1 presents a different trend characterized by a reduction in viscosity of about one order of magnitude in the first region of the curve and an increased gap between the two sweeps, signals of an augmented thixotropy of the system. Similarly TZ2 denotes a stronger reduction in viscosity and a more pronounced difference between the two steps of the analysis. These results clearly suggest a significant impact of Zr (IV) 2,4 pentanedionate in the structural equilibrium of the inks. To better understand this behavior the inks were submitted to rapid changes of shear rate from a steady high shear rate to a lower one, according to Camina – Roffey procedure [23], to study their thixotropic behavior. (Figure 6). Shear rate values were chosen, accordingly to a standard procedure reported in literature, in order to simulate the actual conditions of the screen printing process [22].

P25 and TZ3 samples recover almost completely their initial equilibrium state during the time fixed for the analysis, indicated by the asymptotic trend of the recovery segments; in addition an high similarity between the two curves is confirmed. These results suggest the presence of highly ordered systems as extrapolated by flow curves and prove the absence of interaction between ZrO_2 and TiO_2 surface. On the contrary, ink TZ1 never reach the equilibrium value of viscosity, since its recovery curves does not achieve an asymptotic value of shear stress. This effect, as well as the one observed in the flow curves, could be related to a better dispersion of TiO_2 particles induced by the significant steric hindrance of Zr (IV) 2, 4 pentanedionate, decreasing the viscosity in the whole range of shear rate and increasing the thixotropy of the system. The molecules of precursor could in fact surround TiO_2 particles, creating an additional shell over the already-present dispersant. In such way the dispersion becomes more efficient, in addition the interaction of TiO_2 with the binder is partially screened provoking lower viscosity and structuring of the ink, that enable a slower recovery of the equilibrium conditions and then an higher thixotropy. Concerning ink TZ3, the slope of the recovery curve appears lower than TZ1, indicating a relatively faster restoring of the initial conditions, even if also in this case the asymptote is not reached. This difference may be due to the significantly lower viscosity of the ink, that in this case could accelerate the recovery process since the system is even less rigid and then less perturbed during the analysis. The method by which the precursor is added has therefore a clear impact on the properties of the inks. In the case of TZ2 in fact the mechanisms discussed for TZ1 apparently becomes more efficient. This could be clearly attributed to the functionalization with Zr (IV) 2, 4 pentanedionate before the application of the dispersant, strengthening its dispersing and screening action. Relating to these properties both inks should undergo a better post deposition leveling, inducing an higher

homogeneity of the film with respect to ink P25 and TZ3. A favorable effect of the precursor on the rheological properties of the inks was then pointed out.

In order to collect more information about the effects of the Zr precursor on TiO_2 and to analyze in more detail the effectiveness of the proposed doping method, the inks were calcined to obtain powder samples enabling fundamental characterization such as specific surface area (S.S.A.) determination, XRD analysis and band gap estimation via diffuse reflectance spectroscopy. The calcination was necessary for these analysis to obtain the modified TiO_2 in powder form, since all the processes are conceived to promote the doping only during the sintering of the deposited layer, without intermediate steps. The thermal cycle was conducted at 450°C for 30 minutes, in order to simulate the actual conditions that will be used for the layers.

B.E.T analyses of the three calcined TZ samples did not show any variation in S.S.A. compared to the one of un-calcined P25 (50 ± 15 m^2/g), indicating that neither the relatively low temperature treatment and the presence of Zr additives induced any relevant phenomena of particle agglomeration.

XRD analysis were done to determine the evolution of Zr into the TiO_2 crystal lattice and then to validate the doping procedure. Diffraction patterns of P25, TZ1, TZ2 and TZ3 calcined samples are reported in Figure 7.

X – ray diffraction measurement clearly identified the presence of ZrO_2 in TZ3 as indicated with dotted lines. This result confirms that, for this approach, Zr is not able to diffuse into the crystal lattice of TiO_2 but remains as a secondary phase segregated from TiO_2 particles. On the contrary, no diffraction peaks of ZrO_2 or other phases were

observed for TZ1 and TZ2, sign of an effective incorporation of Zr into the TiO_2 structure [13-15,20,21].

TiO_2 cell parameters are generally supposed to expand in the case of Zr doping due to the difference in ionic radii between the two cations (Zr^{4+} = 72 pm, Ti^{4+} = 61 pm), and/or to the formation of surface defects that balance eventual lattice deformations[21]. However, no relevant changes from the original P25 values were detected, both for anatase (a/b = 4.592 nm, c = 2.958 nm) and rutile (a/b = 3.785 nm, c = 4.592 nm) phase. This evidence could be strictly related to the low quantity of Zr introduced, as already noticed by Lukac and co-workers in 0,8 % mol Zr-doped TiO_2 produced by co-precipitation method [24].

Zr is well known to stabilize the anatase phase of TiO_2 [13-15,20,21,24], therefore it is reasonable to think that if it is effectively inside the crystal lattice, calcining the powder at a temperature higher than the one of the anatase-rutile transition would not affect the phase composition. For this reason each system was calcined at 700°C for 30 minutes. Figure 8 reports the obtained patterns compared with the previous ones.

TZ1 and TZ2 do not show any variations with temperature, no substantial phase transformations has then occurred, nor a Zr migration inside the lattice that was not detected before (the position of the peaks remains unchanged). On the contrary, TZ3 samples clearly exhibit an increased intensity of rutile diffraction peaks, indicating that the phase transition is not hindered since ZrO_2 in the formulation does not enter the crystal lattice of TiO_2. In addition, a slight narrowing of diffraction peaks is observed in TZ3 calcined at 700°C, as a consequence of crystallite growth induced by temperature, while no such modifications are present in the other two samples.

To better analyse these evidences, Rietveld refinement of the obtained patterns was done to quantify the phase composition; in addition the crystal sizes were calculated using the Debye-Scherrer formula (*Eq. 1*).

$$\tau = \frac{K\lambda}{\beta \cos\theta} \qquad (Eq.\ 1)$$

Where τ is the crystal size, K is a shape factor (0.9), λ is the X-ray wavelength, β is the broadening at the FWHM in radians and θ is the Bragg angle. The results are reported in Figure 9 (only anatase data reported).

The trends of anatase phase reported in Figure 8a give a clear indication of the stabilizing action of Zr inside the TiO_2 lattice. As observed from the XRD patterns in fact, the calcination at 450°C did not caused any changes in the phase composition, on the contrary using a process temperature of 700°C, above the anatase-rutile transition, the amount of anatase phase for the pure P25 sample is suppressed at about 50% from the initial 80%. This transition evolved also for TZ3, having he segregated TiO_2 no stabilizing effects. The efficacy of TZ1 and TZ2 procedure is instead proven by the hindering of this phase transformation, the anatase amount was in fact stabilized at about 80%. The same behavior was observed for the crystal size (Figure 8b). Calcining the powders at 700°C induced a significant crystal growth, due to the diffusion through the grains, for P25 and TZ3; while this phenomenon was hindered for TZ1 and TZ2. These effects can be explained by two different mechanisms. First, Zr^{4+} ions may segregate in the grain boundaries of anatase TiO_2, acting as a barrier for the diffusion process at grain contact, necessary for the crystal growth. Secondly Zr^{4+} ions are more electropositive than Ti^{4+} ones, and then they could donate their electron density to O^{2-}. In this way the Ti-O bond becomes more stable and more difficult to break, so the

anatase – rutile phase transformation is hindered [20]. In conclusion, XRD analyses suggested that phase stabilization and inhibition of crystallite growth with increasing temperature could represent the main proves of the effectiveness of TZ1 and TZ2 methods for the doping of TiO_2 [20,21,24].

Another effect on the properties of TiO_2 that is generally attributed to the doping with Zr is the increase of the optical band gap energy, due to the higher band gap of ZrO_2 (≈ 5.0 eV) compared to TiO (≈ 3.0 eV). Moreover, crystal size growth inhibition induced by doping originates quantum confinement effects, thus playing a major role in the band gap increase [13-15,20,21].

Band gap energy (E_g) estimation was therefore performed using a spectrophotometric method [25,26]; diffuse reflectance spectra were collected and converted to F(R) using the Kubelka-Munk equation (*Eq. 2*)

$$F(R) = \frac{(1-R)^2}{2R} \qquad (Eq.\ 2)$$

Where R is the reflectance value collected at any wavelenght

Tauc relationship was then applied for the calculation of the band gap energy (*Eq. 3*)

$$(F(R)h\nu)^{1/n} = A\left(h\nu - E_g\right) \qquad (Eq.\ 3)$$

h is the Planck's constant ($6{,}626 \times 10^{-34}$ J s), A is a proportional constant, *v* is the frequency of vibration (s^{-1}), and the value of the exponent *n* denotes the nature of the electronic transition whose value is different for each kind of transition involved; in this case n = 2 was chosen for TiO_2, indicating indirect allowed electronic transitions. Eg

values were finally obtained by plotting $[F(R)hv]^{1/n}$ vs hv (Tauc plot) and extrapolating the interception between the linear part of the curves and the x axis.

Tauc plots and related Eg values are reported in Figure 10.

The obtained data do not show however any significant variation in E_g values of TZ samples, compared to P25; although different studies have shown that even such a low Zr amount gives an increase of the band gap energy [13,20]. This apparent discrepancy with the literature data could be explained considering the specific doping method introduced in this work.

Quantum confinement effects in fact are basically associated to doping processes developed during the powder synthesis, like sol – gel or co – precipitation methods. In the present case on the other hand, doping occurs on a pre–synthetized commercial powder and the calcination at 450°C did not induce any significant difference in crystal size between P25 and TZ samples, therefore the contribute of the quantum confinement to Eg cannot be considered. Moreover Zr doping might increase the oxygen vacancies concentration: at this low percentage of doping the unexpected levelling of E_g values could therefore be ascribed to the formation of a defect band originated by oxygen vacancies, that overlaps with the conduction band of TiO_2 [21].

3.2 Films characterization

Surface SEM micrographs of the deposited films are reported in Figure 11. Coherently with previous analyses, P25 and TZ3 do not exhibit significant differences and are characterized by a quite inhomogeneous porosity and some particle aggregates. The film quality is slightly improved for TZ1, in which the formation of aggregates is suppressed. Finally, the most relevant improvements are obtained for TZ2, the particle

dispersion is in fact further enhanced and the porosity is fine and homogeneously distributed. These results are in agreement with rheological analysis, that pointed out the significant dispersing action of Zr (IV) 2, 4 pentadionate, reducing the viscosity of the inks. This effect is partially observed for TZ1 film and more evident for TZ2, in fact the respective ink showed the lowest values of viscosity and then the most efficient particles dispersion, due to the direct contact between TiO_2 and the precursor molecules, as discussed in the previous section.

The capability of adsorbing high amounts of sensitizer is one of the main requisites for a semiconductor oxide layer to be used as DSC photoande; for these reason the impact of the different process used on the dye adsorption was studied. The dye uptake was quantified by desorption of the sensitizer (N719) with 0.1 M NaOH aqueous solution. As reported in Table II, P25, TZ1 and TZ3 gave basically the same response, in accordance with the minor differences emerged from the morphological characterization. However this results has another significant implication, that is that the tested doping procedure (TZ1) did not produce modifications of the surface chemistry of TiO_2, not affecting its interaction with the dye molecules. Accordingly to the morphology observed by SEM micrographs, TZ2 films adsorbed a slightly higher amount of sensitizer, due to the larger fraction of TiO_2 surface available for the sensitization.

Table II. Dye N719 0.3 mM loading and Flat band potentials of P25 and TZ series films.

Sample	Dye Loading [10^{-8} mol/cm^2]	E_{FB} [V]
P25	4.6 ± 0.1	-0.69 ± 0.01
TZ1	4.7 ± 0.1	-0.75 ± 0.04

TZ2	5.0 ± 0.1	-0.82 ± 0.02
TZ3	4.6 ± 0.1	-0.72 ± 0.01

The effect of the doping procedure on the morphology of the films, and consequently on the dye adsorption capability, are two fundamental parameters with a strong influence on the overall functioning of a DSC. Considerable attention was given to these properties since they could have been particularly influenced by a significant modification of the process, as the addition of a precursor to the formulation of the screen-printing ink.

Therefore, after having pointed out the interesting correlations between the processes used and the characteristics of the inks and respective deposited layers, and having demonstrated the effectiveness of the TZ1 procedure as a doping method; the following characterizations focused on the electrochemical behavior of TiO_2 and TZ layer were done, in view of their application as DSC photoanodes.

Initially, the band structure of P25 and TZ samples was evaluated through Mott Schottky (MS) analysis, by measuring the space charge capacitance as a function of the electrode potential in depletion conditions. MS relationship is expressed as follow (*Eq. 4*):

$$(C_{sc})^{-2} = \frac{2(E - E_{FB} - \frac{kt}{e})}{N_D \, \varepsilon \varepsilon_0 e A^2} \qquad \textit{(Eq. 4)}$$

Where C_{SC} is the space charge capacity, N_D is the carrier density, ε the relative electric permittivity, ε_0 the electric permittivity of vacuum, e the elementary charge, E the applied potential, E_{FB} the flat band potential, A the active surface, T the absolute temperature and k the Boltzmann constant. The electron density and the flat band

potential of the electrode can be obtained by the slope and the intercept of MS plots ($1/C^2$ vs V), reported in Figure 12.

The E_{FB} values extrapolated from the MS plots are listed in Table II. Compared to P25, TZ1 and TZ2 show a negative shift of the potential, as a consequence of Zr doping. The E_{FB} of TZ3 decreases as well, although previous analysis clarified that in this conditions doping did not occur; however this result could be originated by the presence of ZrO_2 particles. The displacement of E_{FB} observed for TZ1 and TZ2 could have a positive influence for the application in DSCs, in terms of increasing $V_{OC,}$ by enlarging the potential difference between the Fermi level of the TiO_2 photoanode and the electrochemical potential of the electrolyte. No relevant differences were observed in the slopes of MS plots, this is probably coherent with the low amount of dopant used. Therefore, to get more information about the electronics of the films, cyclic voltammetry (CV) analysis were conducted. CV is a well know method for the determination of the density of states (DOS) of nanoporous semiconductors [27,28,29], exploiting the correlation with the electrochemical capacitance of the studied material. The capacitance (C) is proportional to the current (i) according to the following equation (Eq. 5):

$$\boldsymbol{i = dq/dt = C\, dU/dt = Cv} \qquad \textit{(Eq. 5)}$$

Where q is the elementary charge, t the time, U the potential, and v the scan rate. At constant scan rate, a direct relationship exists between current intensity and DOS, expressed by the value of C. Figure 13 reports the cyclic voltammograms of the studied samples.

Each TZ sample exhibits a larger faradic current compared to the P25 reference electrode. The peak of TZ2 appears very similar to the TZ3 one, even though in the latter this effect could be again related to the presence of segregated ZrO_2 phase. TZ1 shows the larger current peak and consequently the higher increase in DOS. Such a modification could mean an enhanced electrode capability of accepting electrons, with resulting benefits on the rate of the electron transfer and then finally on the performances of the cell.

In addition, only TZ1 voltammogram registered a small intensity peak located at more positive potentials than the faradic one, as shown in the inset in Figure 13. This evidence has been related to an increased amount of electronic surface states [27], that in the present case could be originated by Zr doping. In DSCs, surface state are supposed to improve the electrical conductivity of the photoanode and the interfacial electron transfer between TiO_2 and FTO [30]. Nonetheless it is known that surface states can act as trap states for electron recombinations [3]. The effective tuning of the doping of TiO_2 will be therefore fundamental to optimize the properties of the photoanode in order to maximize the improvements deriving from this novel procedure.

4. Conclusions

The present work reported the study of a novel approach for the doping of TiO_2 with Zr^{4+}. The process, identified with the sample TZ1, involved the addition of a specific precursor, Zr (IV) 2, 4 pentanedionate), directly to the solvent of the screen-printing ink used for the deposition of ceramic layers, functioning as photoanodes in DSCs. An impregnation – like process (TZ2) and a mixture of TiO_2 and ZrO_2 nanopowders (TZ3) were also realized for comparison, in order to analyze different methods for the doping of TiO_2 through the modification of a screen-printing ink formulation.

The insertion of Zr^{4+} ions into TiO_2 crystal lattice was proved by XRD analyses, pointing out the anatase phase stabilization and the crystal growth inhibition at high temperature (700°C), both for TZ1 and TZ2. On the contrary, the powder mixture of ZrO_2 and TiO_2 did not originate significant interaction between the oxides. Rheological measurements evidenced a strong impact of the Zr precursor on the behavior of the inks, probably due to a steric dispersing action; further studies are currently under investigation in order to examine more in depth this phenomenon.

Analysis on the screen printed films were conducted to evaluate the potential application of this process for the realization of efficient DSC photoanodes. Morphology of TZ1 films was found to be slightly improved, compared to the P25 ones; the presence of particle aggregates was in fact reduced. Moreover the dye adsorption capability remained basically constant, indicating that the doping procedure was successfully completed without reducing the chemical affinity between TiO_2 and N719. Concerning the electrochemical behavior of the films, flat band potential and density of states (DOS) resulted to increase as a consequence of Zr doping, with possible benefits on the V_{OC} of a complete device and on the interfacial electronic transfer, respectively. The development of this work forecasts operation tests in order to evaluate the achievement of an effective performance enhancement, different dopant concentration will be considered as well to get a deeper knowledge about the versatility of the procedure. In conclusion, this paper introduced an alternative route for the rapid and efficient doping of TiO_2 with Zr^{4+}, applied to the realization of screen-printed DSC photoanodes, that is potentially transferable to other other dopant – semiconductor systems.

Acknowledgments

....

References

[1] B. O'Regan, M. Gratzel, A low cost, high-efficiency solar cell based on dye-sensitized colloidal TiO_2 films, Nature 353 (1991) 737-739.

[2] S. Mathew, A. Yella, A. Yella, P. Gao, R. Humphry-Baker, B. F. E. Curchod, N. Ashari-Astani, I. Tavernelli, U. Rothlisberger, Md. K. Nazeeruddin and M. Graetzel, Dye-sensitized solar cells with 13% efficiency achieved through the molecular engineering of porphyrin sensitizers, Nature Chemistry 6 (2014) 242–247.

[3] A. Hagfeldt, G. Boschloo, L. Sun, L. Kloo, H. Petterson, Dye-sensitized solar cells, Chem. Rev. 110 (2010) 6595–6663.

[4] R. Jose, V. Thavasi and S. Ramakrisha, Metal oxides for dye-sensitized solar cells, J. Am. Ceram. Soc. 92 (2009) 289-301.

[5] T. Ma, M. Akiyama, E. Abe, I. Imari, High-efficiency dye-sensitized solar cell based on a nitrogen-doped nanostructured titania electrode, Nano Lett. 5 (2005)2543-2547.

[6] S. Yang, S. Guo, D. Xu, H. Xue, H. Kou, J. Wang, G. Zhu, Improved efficiency of dye-sensitized solar cells applied with F-doped TiO_2 electrodes, Journal of Fluorine Chemistry 150 (2013) 78-84.

[7] Q. Liu, Y. Zhou, Y. Duan, M. Wang, X. Zhao, Y. Lin, Enhanced conversion efficiency of dye-sensitized titanium dioxide solar cells by Ca-doping, Journal of Alloys and Compounds 548 (2013) 161-165.

[8] H. Tian, L. Hu, C. Zhang, L. Mo, I. Sheng, L. Mo, W. Li, Enhanced photovoltaic performance of dye-sensitized solar cells using a highly crystallized mesoporous TiO2 electrode modified by boron doping, J. Mater. Chem, 21 (2011) 863-868.

[9] K. P. Wang, H. Teng, Zinc-doping in TiO_2 films to enhance electron transport in dye-sensitized solar cells under low-intensity illumination, Phys. Chem. Chem. Phys, 11 (2009) 9489-9496.

[10] S. Iwamoto, Y. Sutanami, M. Inoue, T. Hoshi, K. Shigaki, M. Kaneko, A. Maenosono, Charge recombination and band-edge shift in dye-sensitized Mg^{2+}-doped TiO_2 solar cells, J. Phys. Chem. C 115 (2011) 16418-16424.

[11] Y. Duan, N. Fu, Q. Liu, Y. Fang, X. Zhou, J. Zhang, Y. Lin., Sn-doped TiO_2 photoanode for dye-sensitized solar cells, J. Phys. Chem. C 116 (2012) 8888-8893.

[12] A. K. Chadiran, F. d. r. Sauvage, M. Casas – Cabanas, P. Comte, S. M. Zakeerudin, M. Graetzel. Doping a TiO_2 photoanode with Nb^{5+} to enhance transparency and charge collection efficiency in dye-sensitized solar cells, J. Phys. Chem, C 114 (2010) 15849-15856.

[13] M. Durr, S. Rosselli, A. Yasuda, G. Nelles, Band-Gap engineering of metal oxides for dye-sensitized solar cells, J. Phys. Chem. B 110 (2006) 21899-21902.

[14] S. Kim, M. Kang, Band gap tuning in nanoporous TiO_2-ZrO_2 hydbrid thin films, Bull. Korean Chem. Soc. 32 (2011) 3317-3322.

[15] A. Kitiyanan, S. Ngamsinlapasathian, S. Pavasupree, S. Yoshikawa, The preparation and characterization of nanostructured TiO_2-ZrO_2 mixed oxide electrode for efficient dye-sensitized solar cells, Journal of Solid State Chemistry 178 (2005) 1044-1048.

[16] D. Menzies, R. Cervini,, Y. Cheng, P Simon, L. Spiccia, Nanostructured ZrO_2-coated TiO_2 electrodes for dye-sensitized solar cells, Journal of Sol – Gel Science and Technology 32 (2004) 363-366.

[17] G. Dell'Agli, C. Ferone, G. Mascolo, M. Pansini, Crystallization of monoclinic zirconia from metastable phases, Solid State Ionics 127 (2000) 223-230.

[18] S. Petit, S. Morlens, Z. Yu, D. Luneau, G. Pilet, J. Soubeiroux, P. Odier,Synthesis and thermal decomposition of a novel zirconium acetate-propionate cluster: [Zr12], Solid State Science 13 (2011) 665-770.

[19] M. Piquart, T. Lopez, R. Gomez, E. Torres, A. Moreno and J. Garcia, Dehydration and crystallization process in sol-gel zirconia, Journal of Thermal Analysis and Calorimetry 76 (2004) 755-761.

[20] N. Venkatachalam, M. Palanichamy, B. Arabindoo, V. Murugesan, Enhanced photocatalytic degradation of 4-chlorophenol by Zr^{4+} doped nano TiO_2, Journal of Molecular Catalysis A: Chemical 266 (2007) 158-165.

[21] J. Lukac, M. Klementoca, P. Bezsdicka, S. Bakardjieva, J. Subrt, L. Szatamary, Z. Bastl, J. Jirkovsky, Influence of Zr as TiO_2 doping ion on photocatalytic degradation of 4-chlorophenol, Applied Catalysis B: Environmental 24 (2007) 89–91.

[22] A. Sanson, D. Gardini, G. Montanari, C. Galassi, E.Roncari, Key role of milling in the optimization of TiO_2 nanoinks, Journal of Materials Research 21 (2006) 1561-1569.

[23] N. Camina, C. G. Roffey, Statistical interpretation of viscoelasticity, Rheol. Acta 10 (1971) 606.

[24] P. Goswami and J. N. Ganguli, Tuning the band gap of mesoporous Zr-doped TiO_2 for effective degradatation of pesticide quinaphost, Dalton Trans. 42 (2013) 14480-14490.

[25] R.López, R.Gómez, ,Band-gap energy estimation from diffuse reflectance measurements on sol-gel and commercial TiO_2: a comparative study, Journal of Sol-Gel Science Technology 61 (2012) 1 -7.

[26] J. Li, Y.Cai Zhang, M.Zhang, Low temperature preparation and optical properties of $K_2Ti_6O_{13}$, Materials Letters 79 (2012) 136-138.

[27] J. Bisquert, F. Fabregat-Santiago, I. Mora-Sero, G. Garcia-Belmonte, E. M. Barea, E. Palomares, A review of recent results on electrochemical determination of the density of electronic states of nanostructured metal-oxide semiconductors and organic hole conductors, Inorganica Chimica Acta 361 (2008) 684-698.

[28] J. Bisquert, Chemical capacitance of nanostructured semiconductors: its origin and significance for nanocomposite solar cells, Phys. Chem. Chem. Phys. 5 (2003) 5360-5364.

[29] F. Fabregat-Santiago, I. Mora-Sero, G. Garcia-Belmonte and J. Bisquert, Cyclic voltammetry studies of nanoporous semiconductors. Capacitive and reactive properties of nanocrystalline TiO_2 electrodes in aqueous electrolyte, J. Phys. Chem. B, 107 (2003) 758-768.

[30] J. Akilavasan, K. Wijeratne, H. Moutinho, M. Al-Jassim, A. R. M. Alamoud, R. M. G. Rajapkse and J. Bandara, Hydrothermally synthesized titania nanotubes as a promising electron transport medium in dye sensitized solar cells exhibiting a record efficiency of 7.6% for 1- based devices, J. Mater. Chem. A, 1 (2013) 5377-5385.

Figure captions

Figure 1 – Zr(IV) 2, 4 pentanedionate structure formula.

Figure 2 - TG/DSC curves of Zr(IV) 2,4 pentanedionate.

Figure 3 – TZ inks preparation procedure.

Figure 4 – TG/DSC curves of ink TZ1.

Figure 5 – Flow curves of P25 and TZ inks.

Figure 6 – Thixotropic behavior of P25 and TZ inks.

Figure 7 – XRD patterns of P25 and TZ samples calcined at 450°C for 30 minutes.

Figure 8 – XRD patterns of TZ samples calcined at 450°C (dotted lines) and 700°C (continuous lines) for 30 minutes.

Figure 9 – a) Anatase phase composition and b) anatase crystal size of P25 and TZ samples calcined at 450°C and 700°C for 30 minutes.

Figure 10 – Tauc plots and Eg values (inset) of P25 and TZ samples.

Figure 11 – Surface FE-SEM micrographs of P25 and TZ films.

Figure 12 – Mott Schottky plots of P25 and TZ films.

Figure 13 – Cyclic voltammograms of P25 and TZ films (scan rate 10 mV s^{-1}). The last of five scans is reported for each sample.

Figure 1

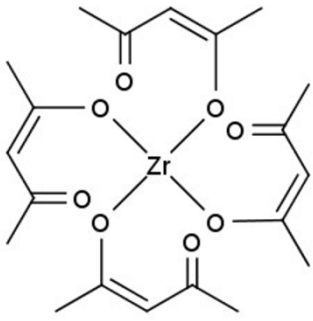

Figure 2

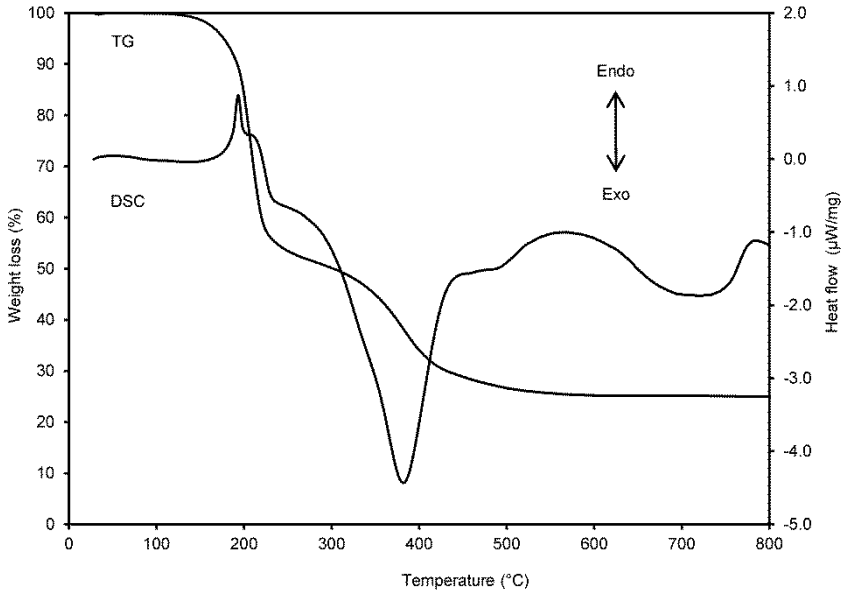

Figure 3

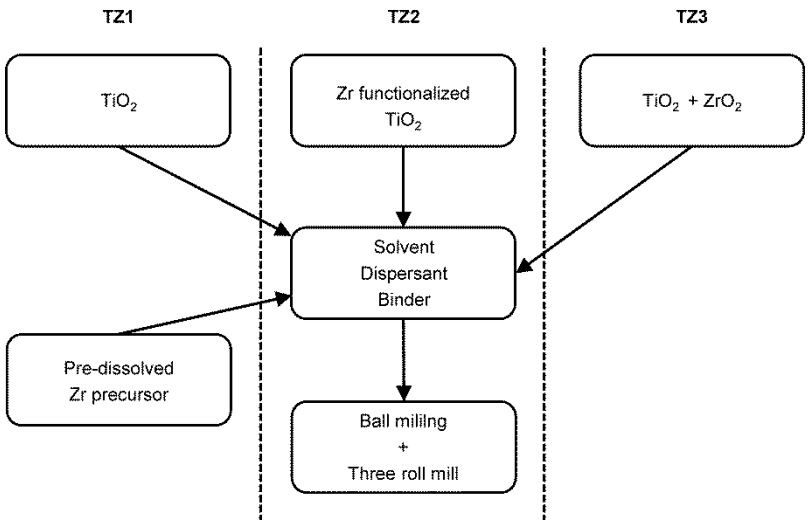

Figure 4

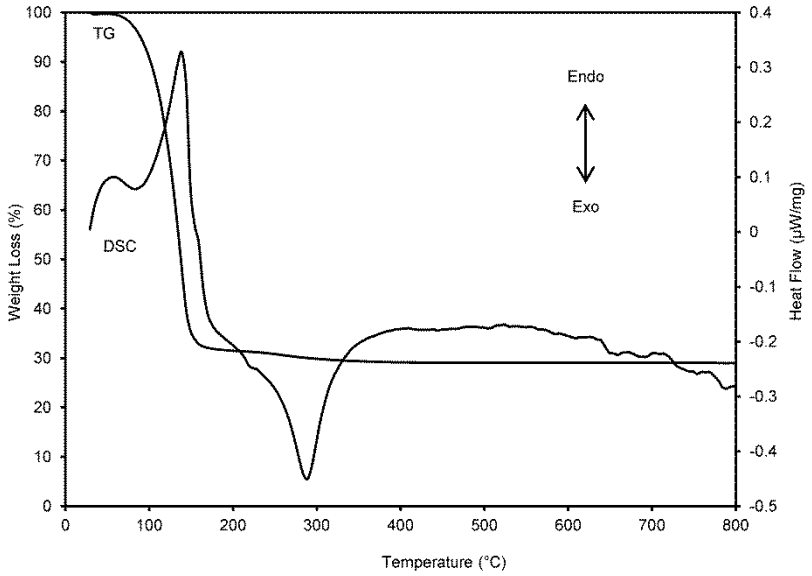

Figure 5

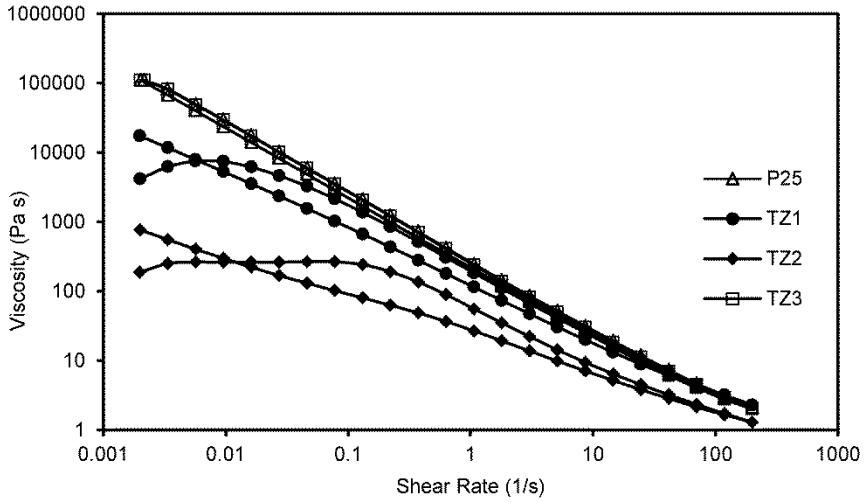

Figure 6

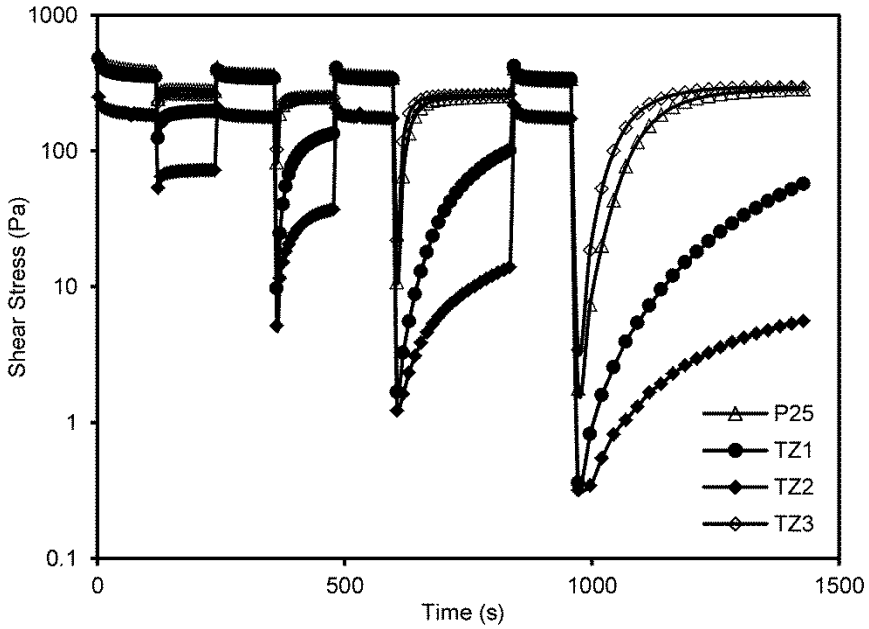

Figure 7

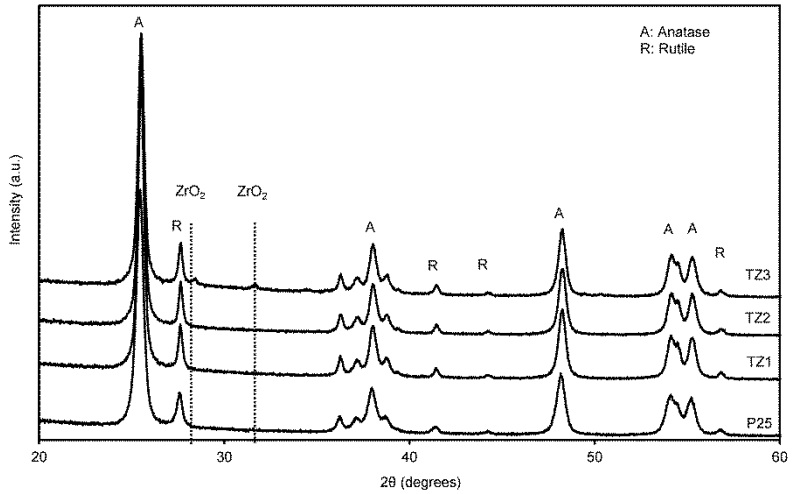

Figure 8

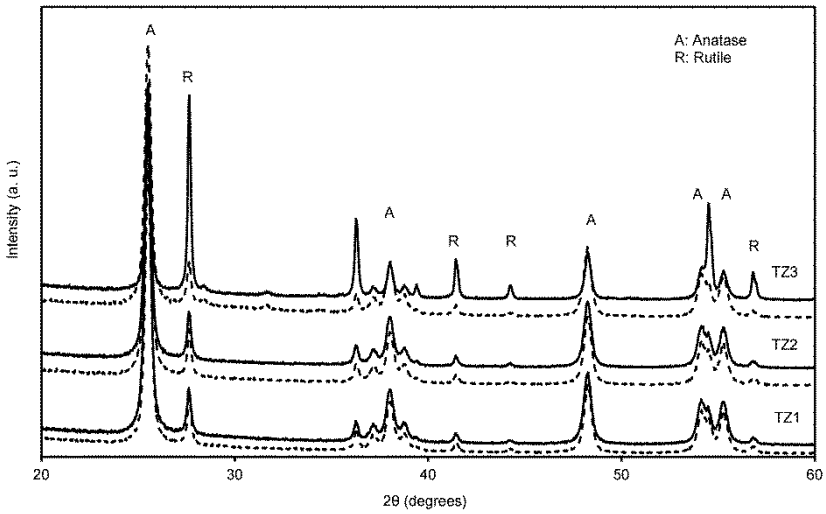

Figure 9

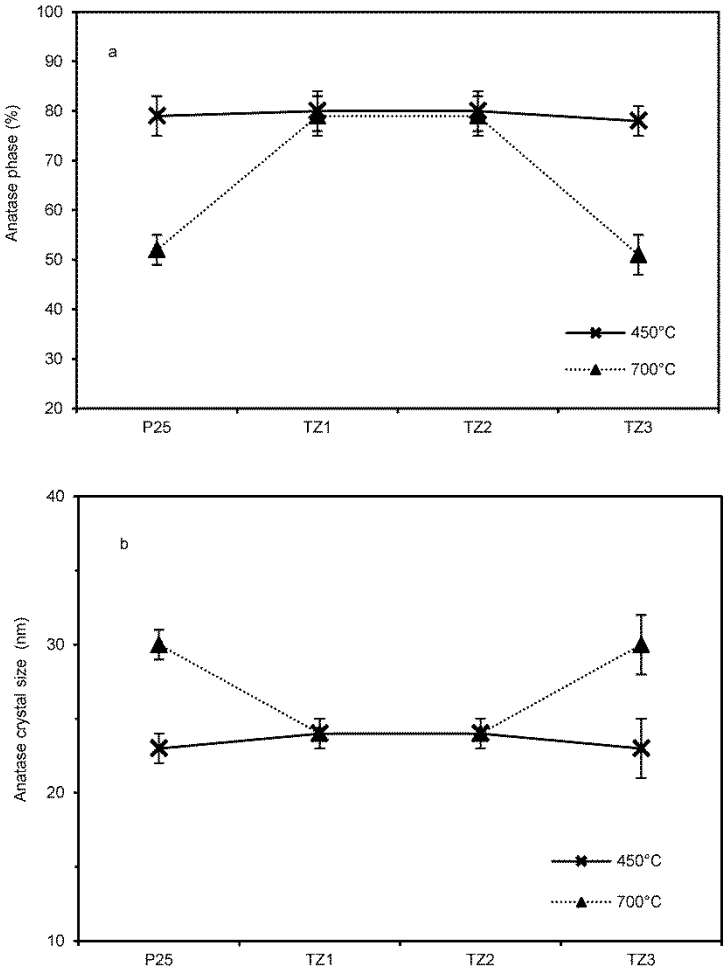

Figure 10

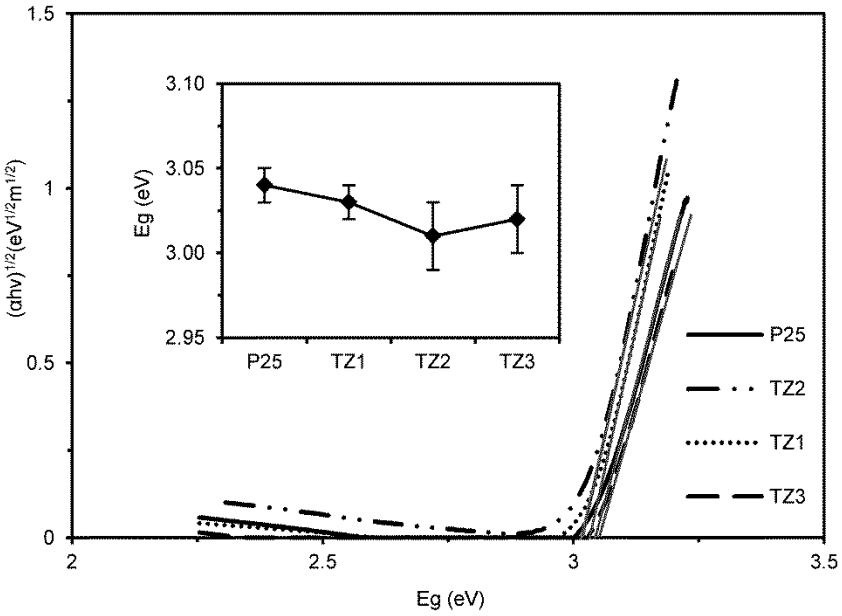

Figure 11

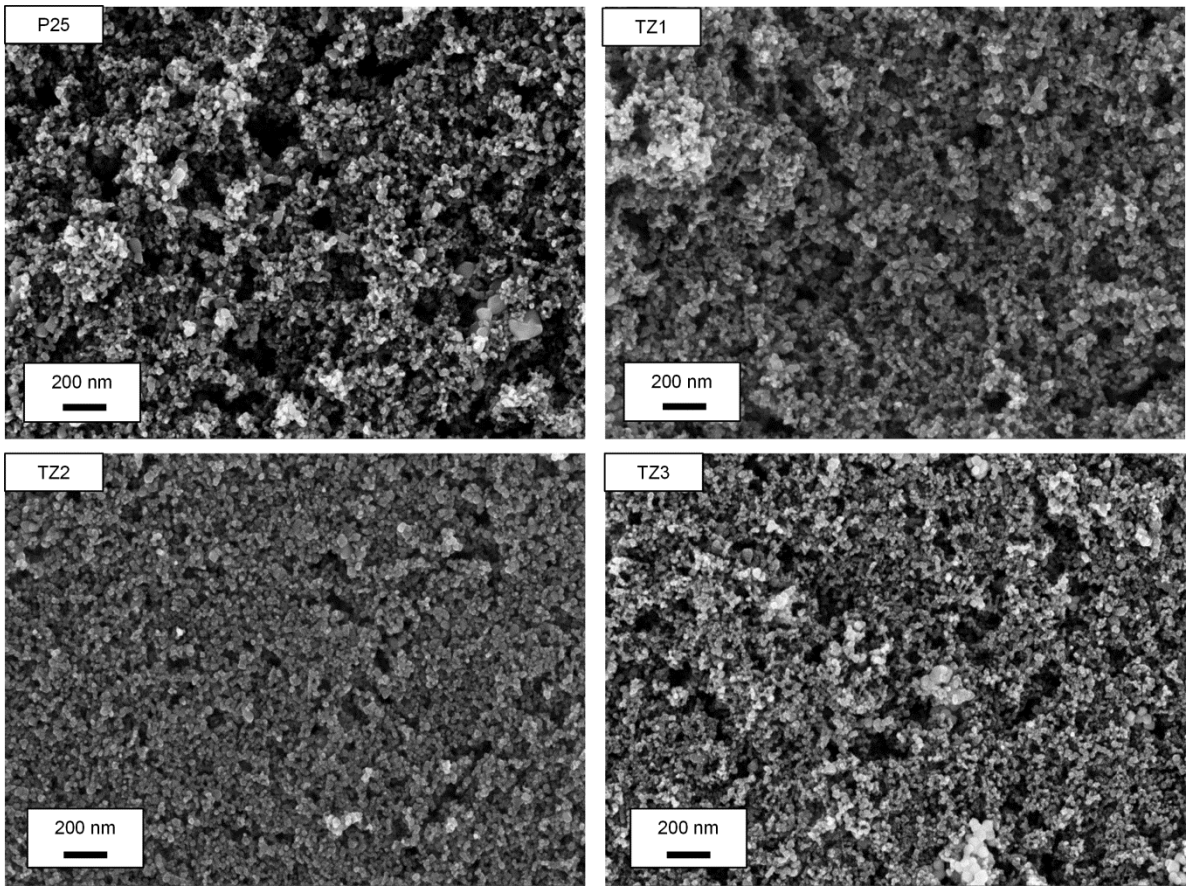

Figure 12

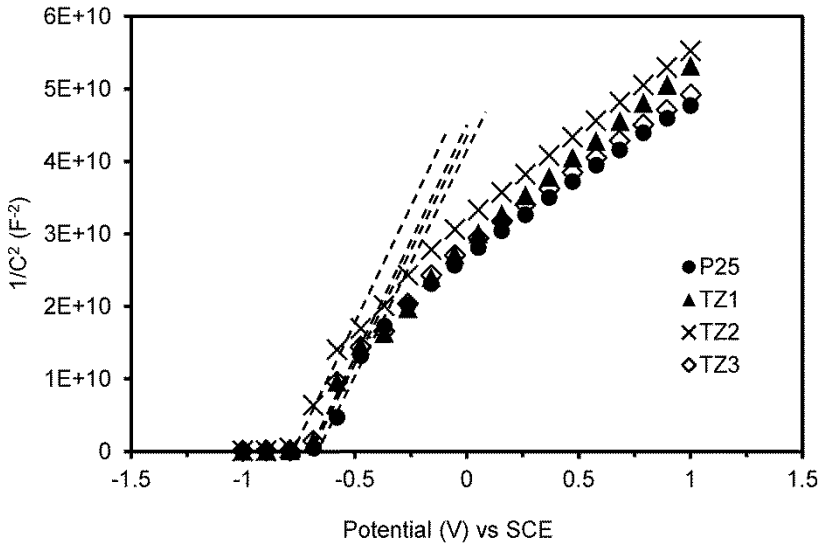

Figure 13